

Prediction of dual agents as an activator of mutant p53 and inhibitor of Hsp90 by docking, molecular dynamic simulation and virtual screening



Maryam Abbasi^{a,b}, Hojjat Sadeghi-Aliabadi^a, Farshid Hassanzadeh^a, Massoud Amanlou^{b,*}

^a Department of Medicinal Chemistry, Faculty of Pharmacy, Isfahan University of Medical Sciences, 81746-73461 Isfahan, Iran

^b Department of Medicinal Chemistry, Faculty of Pharmacy, Pharmaceutical Science Research Center, Tehran University of Medical Science, Tehran, Iran

ARTICLE INFO

Article history:

Received 13 February 2015

Received in revised form 2 August 2015

Accepted 3 August 2015

Available online 4 August 2015

Keywords:

Docking

Dual agent

Hsp90 inhibitors

Molecular dynamic simulations

P53

Virtual screening

ABSTRACT

Heat shock protein90s (Hsp90s) play a crucial role in the development of cancer, and their inhibitors are a main target for tumor suppression. P53 also is a tumor suppressor, but in cancer cells, mutations in the p53 gene lead to the inactivation and accumulation of protein. For instance, the ninth p53 cancer mutation, Y220C, destabilizes the p53 core domain. Small molecules have been assumed to bind to Y220C DNA-binding domain and reactivate cellular mutant p53 functions. In this study, one of the mutant p53 activators is suggested as an Hsp90 inhibitor according to a pyrazole scaffold. To confirm a new ligand as a dual agent, molecular docking and molecular dynamic simulations were performed on both proteins (p53 and Hsp90). Molecular dynamic simulations were also conducted to evaluate the obtained results on the other two pyrazole structures, one known as Hsp90 inhibitor and the other as the reported mutant p53 activator. The findings indicate that the new ligand was stable in the active site of both proteins. Finally, a virtual screening was performed on ZINC database, and a set of new dual agents was proposed according to the new ligand scaffold.

© 2015 Published by Elsevier Inc.

1. Introduction

Heat shock proteins (Hsps) are molecular chaperones which contribute to the appropriate folding and the function of many proteins [1,2]. Hsps are classified into families by their molecular weights: Hsp100, 90, 70, 60, 40, and small Hsps [3]. Of these families, Hsp90 specifically facilitates the folding of the nascent proteins (client proteins) by interacting with a set of auxiliary proteins (co-chaperones).

Hsp90 contains three main domains: the N-terminal ATP-binding domain, the middle region domain and the C-terminal domain. The function of the Hsp90 dimer is affiliated to its binding capability and hydrolysis of ATP [4]. More than 200 proteins, such

as protein kinases, nuclear steroid receptor, telomerase, p53 and tubulin are folded by Hsp90 in order to reach their firm and active conformational state [5–7]. Many of them are directly attributed to oncogenes. Among these, p53 has a greater significance because of its unique role in tumor suppression. Fig. 1 briefly depicts the role of Hsp90 in the growth of tumor cells.

The p53 transcription factor is a tetrameric multidomain protein, which includes a N-terminal transactivation domain, DNA-binding domain, tetramerization domain, and C-terminal regulatory domain [8]. The concentration of p53 is maintained at an extremely low level in normal cells, but it is activated and stabilized as a transcription factor in the cells under stress [9]. In cancer cells, p53 induces both cell cycle arrest and apoptosis by expression of p21WAF1, gadd45 and other proteins, so it inhibits proliferation of damaged cells [10].

In 55% of human tumors, the p53 gene mutates, which leads to inactivation and accumulation of p53 [11]. The majority of human tumor p53 mutations are missense mutations in their DNA-binding (core domain). They can be divided into two groups: DNA-contact mutations and structural mutations. In the DNA-contact mutations, the residues which are involved in interference between p53 and DNA change, and in the structural mutations, those residues

Abbreviations: Hsp90, heat shock protein90; MDs, molecular dynamic simulations; Rg, radius of gyration; RMSD, root mean square deviation; RMSF, root mean square fluctuation; VS, virtual screening.

* Corresponding author. Fax: +98 21 64121111.

E-mail addresses: mabbasi@pharm.mui.ac.ir (M. Abbasi), sadeghi@pharm.mui.ac.ir (H. Sadeghi-Aliabadi), amanlou@tums.ac.ir (M. Amanlou).

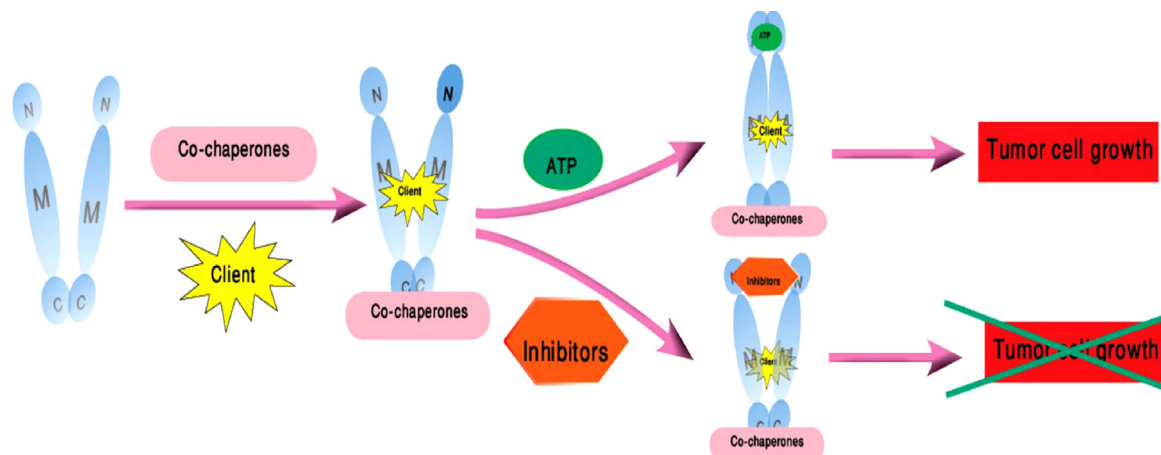


Fig. 1. The role of Hsp90 in the growth of tumor cell. The client protein and co-chaperones bind to Hsp90 in the open state of protein. ATP bind to N-terminal and Hsp90 is closed. ATP is hydrolyzed, the complex changes, client protein is folded and tumor cells grow. Hsp90 inhibitors bind to the N-terminal ATP-binding pocket and thereby the growth of tumor cells is stopped.

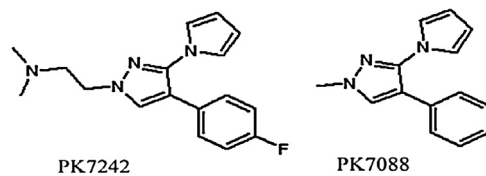


Fig. 2. The chemical structure of the two activators of mutant p53. The chemical structure pyrazole derivatives (PK7242 and PK7088) that reactivate mutant p53 functions.

which are important for keeping the structural stability of the DNA-binding domain undergo a change [12]. In the case of cancer, 30–40% of p53 mutations are of structural type which leads to unfolding and aggregation of the p53 structure at physiological conditions. The ninth most frequent p53 cancer mutation, Y220C, makes a surface cavity that destabilizes the p53 core domain by almost 4 kcal/mol [13,14]. Liu et al. proposed new small molecules (PK7242 and PK7088) that bind to Y220C DNA-binding domain and reactive cellular p53 functions (Fig. 2) [14].

In addition to p53 activators, the pyrazole scaffold also has been seen in Hsp90 inhibitors (Fig. 3). In recent years, considerable attention has been paid to Hsp90 because of its crucial role in the evolution and development of cancer. Hsp90 inhibitors as a significant strategy in cancer therapy include several chemical categories such as isoxazole, pyrimidine, aminoquinolines, arylsulfonamides [15] and pyrazole [16,17].

In this study, a collection of computational procedures were engaged to obtain a new set of compounds that act as dual agents (Hsp90 inhibitor and mutant p53 activator). At the beginning, the docking procedure was validated. After the investigation of

the interaction between PK7242 and Hsp90, a new ligand was predicted. Afterwards, a molecular dynamic simulation (MDs) was conducted to certify the stability of the new ligand in the dynamic environment. This was then compared with the MDs of the activator of mutant p53 (PK7242). MD simulations were performed on inhibitor 2 and the new ligand with Hsp90, and also a comparison was made between them. Finally, in order to predict a set of new dual agents of this category, virtual screening (VS) was conducted on a ZINC database [18] which had a 70% similarity with the new ligand.

2. Material and methods

2.1. Docking simulation studies

All of the input files were prepared by AutoDockTools 1.5.6 package [19]. The pdb file of proteins was taken from the Protein Data Bank (PDB of p53: 3ZME, PDB of Hsp90: 3OWD). All water molecules, except for the water molecules which are important in interactions between protein and ligand, were removed from the protein pdb file as well as all the other heteroatoms such as ligands and ions. After adding polar hydrogens, the partial atomic charge was calculated by Kollman method [20] and it was then saved in the pdbqt format. The pdbqt file, as the input file was rendered to AutoDockTools. For as much as, in both of the proteins (p53 and Hsp90), the water molecules are important in interactions between the protein and ligand, parameters of the water molecules were added to AD4-bound and AD4-parameter files. A $90 \times 90 \times 90 \text{ \AA}$ (x , y , and z) grid box was developed on the macromolecule binding pocket with a 0.375 nm spacing for each dimension. According to the most important residue in the interactions between the ligand

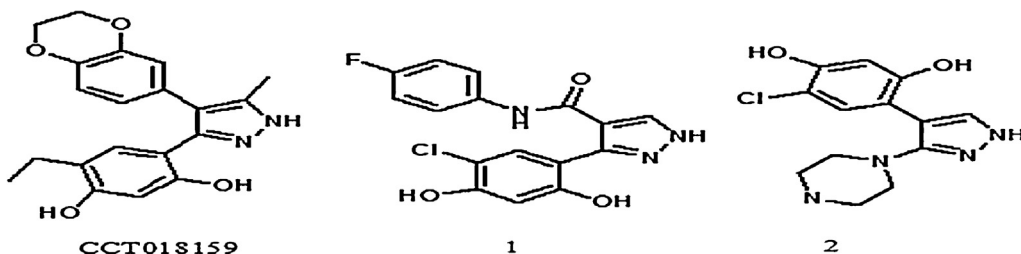


Fig. 3. The chemical structure of the three Hsp90 pyrazole inhibitors. The chemical structure of the discovered pyrazole inhibitors of Hsp90. CCT018159 ($\text{IC}_{50} = 8.9 \mu\text{M}$), inhibitor 1 ($\text{IC}_{50} = 5.35 \mu\text{M}$) and inhibitor 2 ($\text{IC}_{50} = 2 \mu\text{M}$).

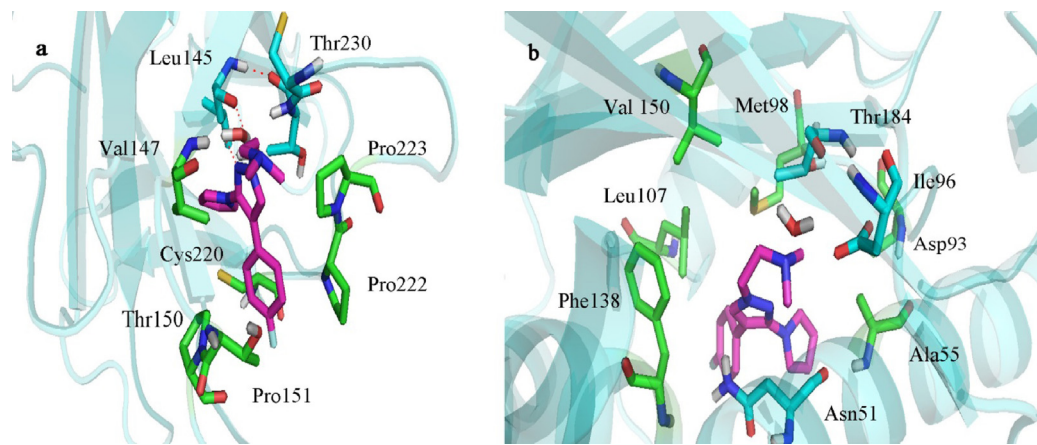


Fig. 4. Molecular docking of the PK7242 ligand with two proteins (p53, Hsp90). (a) Residues involved in the interaction of PK7242 with p53. (b) Residues involved in the interaction of the PK7242 ligand with Hsp90.

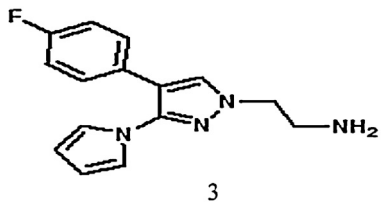


Fig. 5. A proposed new ligand. The new ligand was proposed after docking of PK7242 ligand with p53 and Hsp90.

and protein, the center of the grid was selected and grid maps were created by Autogrid 4.2 [21].

Three-dimensional structures of ligands were drawn in Marvin Sketch v5.7, ChemAxon [22] and were saved in mol2 format. An atomic charge was determined according to Gasteiger-Marsili charge [23].

Docking calculation parameters were specified as the following: number of Lamarckian job = 100, initial population = 150, maximum number of energy evaluation = 25×10^5 , and the default values of other parameters were kept unchanged. Eventually, the docking procedure was carried out by AutoDock 4.2. All of the runs were ranked by the lowest binding energy and were analyzed to obtain the best conformation and orientation of the ligand in the active site of the protein. The ligand-protein interactions were analyzed and visualized by AutoDockTools 1.5.6 and PyMOL Tcl.

2.2. Molecular dynamic simulation

All molecular dynamic simulations of ligand-protein complexes and the analysis of trajectory files were performed with the GROMACS 5.0.5 package [24]. All ligand topology parameters were obtained by the PRODRG web server [25]. The best docking conformation in terms of the binding energy and the orientation in the active site was chosen for the initial direction of the ligand to the protein. Charges in the ligand topology file were edited by Gaussian98 program [26]. The pK_a was calculated by the PROPKA 3.1 web server to determine which residue was more likely to adopt non-standard ionization states [27]. The main structural water molecules in the active site were kept [28]. Protein topology parameters were obtained by the GROMOS96 53a6 force field as well as the simple point charges (SPC) water model. The ligand-protein complex was immersed in a dodecahedron box with a minimum distance of 1 nm between the protein surface and the box boundary, consisting of about 8188 and 8770 solvent molecules in Hsp90 and p53, respectively. The system net charge was neutralized by replacing solvent water molecules with counter ions, Na^+ in Hsp90 and Cl^- in p53. To release spatial clashes of the complex, the energy minimization was performed. First, water molecules were minimized by using 10,000 steepest descents steps; ligand and ions were kept fixed at their initial configuration. Then, the whole system was minimized. This was followed by an MD simulation which included an equilibration stage (NVT and NPT) and a production stage. The NVT step was performed by a 500 ps MD run to equilibrate the system at a constant temperature of 300 K and with a

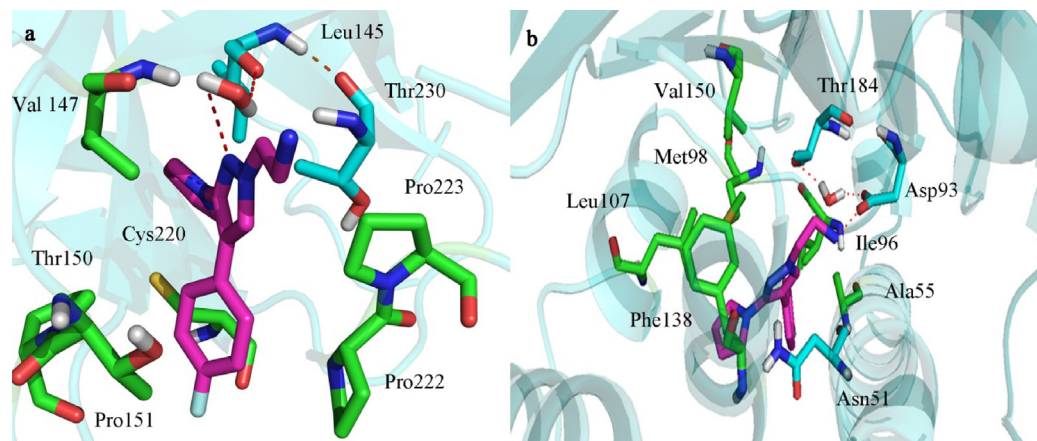


Fig. 6. The main hydrophobic and hydrophilic interactions. (a) The interaction of ligand 3 with p53. (b) The interaction of ligand 3 with Hsp90.

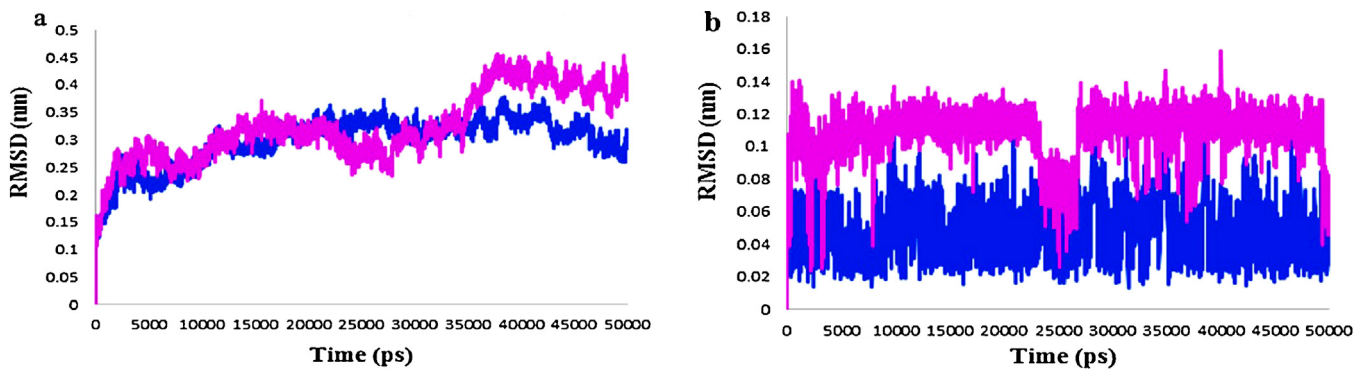


Fig. 7. The RMSD profile. (a) p53 backbone in complex with PK7242 (magenta), ligand 3 (blue). (b) PK7242 (magenta), ligand 3 (blue) as a function of simulation time. (For interpretation of the references to color in this figure legend, the reader is referred to the web version of this article.).

coupling constant of $\tau_T = 0.1$ ps. The temperature was held by the V-Rescale algorithm. After the stabilization of temperature, an NPT ensemble was performed with a coupling constant of $\tau_p = 1$ ps and time duration of 1 ns. Eventually, the system was subjected to an MD production run at 1 bar pressure, an integration step of 2 fs and 100 K, 200 K and 300 K temperatures for 1 ns, 2 ns and 50 ns, respectively. Long-range electrostatic interactions were obtained with the Particle Mesh Ewald (PME) method. The linear constraint (LINCS) algorithm was applied for covalent bond constraints. Furthermore, structure visualization was performed using VMD 1.8.6, PyMOL Tcl and LigPlot + v.1.4.5.

2.3. Virtual screening

Similar compounds of the new ligand from ZINC database (www.zinc.docking.org) were obtained (2150 compounds) [18,29]. The virtual docking experiments were separately performed on p53 and Hsp90 by AutoDock 4.2. First, all of the results were sorted by the binding energy and then the previously reported methods were used to extract the best ligands in the active site of the two proteins.

3. Results and discussion

3.1. Docking simulation analysis

The validation process of the docking method was performed by the docking of PK7242 ligand with p53 and its interactions and positions were compared with the crystallographic poses in PDB: 3ZME. The binding pocket of PK7242 was situated as the following: the pyrazole ring sat in the center of the pocket, and Val147, Thr150 and Pro151 were in one side, and Pro222 and Pro223 were in

the other side of the pocket. Cys220 perched between the phenyl and the pyrrole moiety in the bottom of the packet, and a stabilized structural water molecule by Leu145 and Thr230 formed a hydrogen bond [14].

In all of the docking poses, main interactions between ligand and p53 were seen. The distance between the pyrazole nitrogen atom and the crystallographic water, and Leu145 and the same water was 3.21 Å and 3.29 Å, respectively. Hydrogen bonds are depicted in Fig. 4a. The root mean-square deviation (RMSD) between the valid conformations and their crystal conformation was found to be 1.95 Å. All of the cases above corroborate the reliability of docking for offering a new activator of mutant p53.

Crystallographic file (PDB: 30WD) with a 1.63 Å resolution was chosen for Hsp90. The validation test was done. The binding pocket included a hydrophobic moiety (Ala55, Ile96, Met98, Leu107, Phe138 and Val150), a hydrophilic moiety (Asn51, Asp93 and Thr184), and structural water molecules [30].

The PK7242 ligand was docked with the Hsp90 protein in order to determine this ligand as an Hsp90 inhibitor. 100 docking modes were generated between the PK7242 ligand and Hsp90. All of the 100 docked poses were ranked by their lowest docking energy and were analyzed to obtain the best conformation and orientation of the ligand in the active site. The analysis of all docked poses showed that the PK7242 ligand was located in the binding pocket. Hydrophobic contacts were observed between the residues Ala55, Met98, Leu107 and Gly135, but hydrogen bonds between the ligand Asp93, and a structural water molecule could not be found despite the distance between the terminal amine and Asp93 was 3.12 Å (Fig. 4b). The dimethyl-amine moiety was located near Asp93, but due to the lack of a donor hydrogen group, it could not form a hydrogen bond. To resolve this deficiency, a new ligand (3) was proposed, and the amino group was replaced with the dimethyl-amine moiety (Fig. 5).

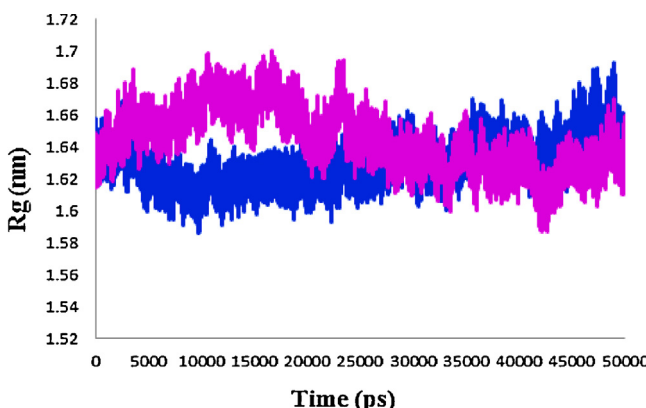


Fig. 8. The gyration radius plot of backbone. P53-PK7242 (magenta) and p53-ligand 3 (blue) complexes.

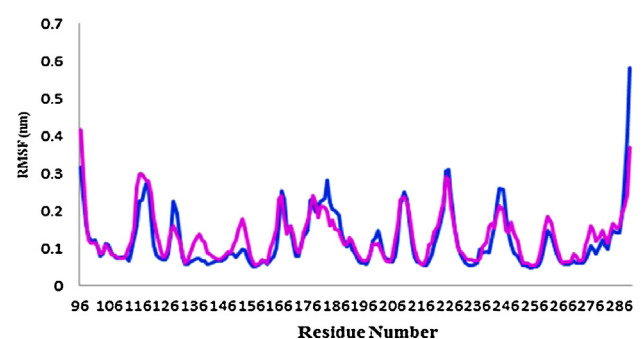


Fig. 9. The RMSF plot. p53-PK7242 (magenta) and p53-ligand 3 (blue).

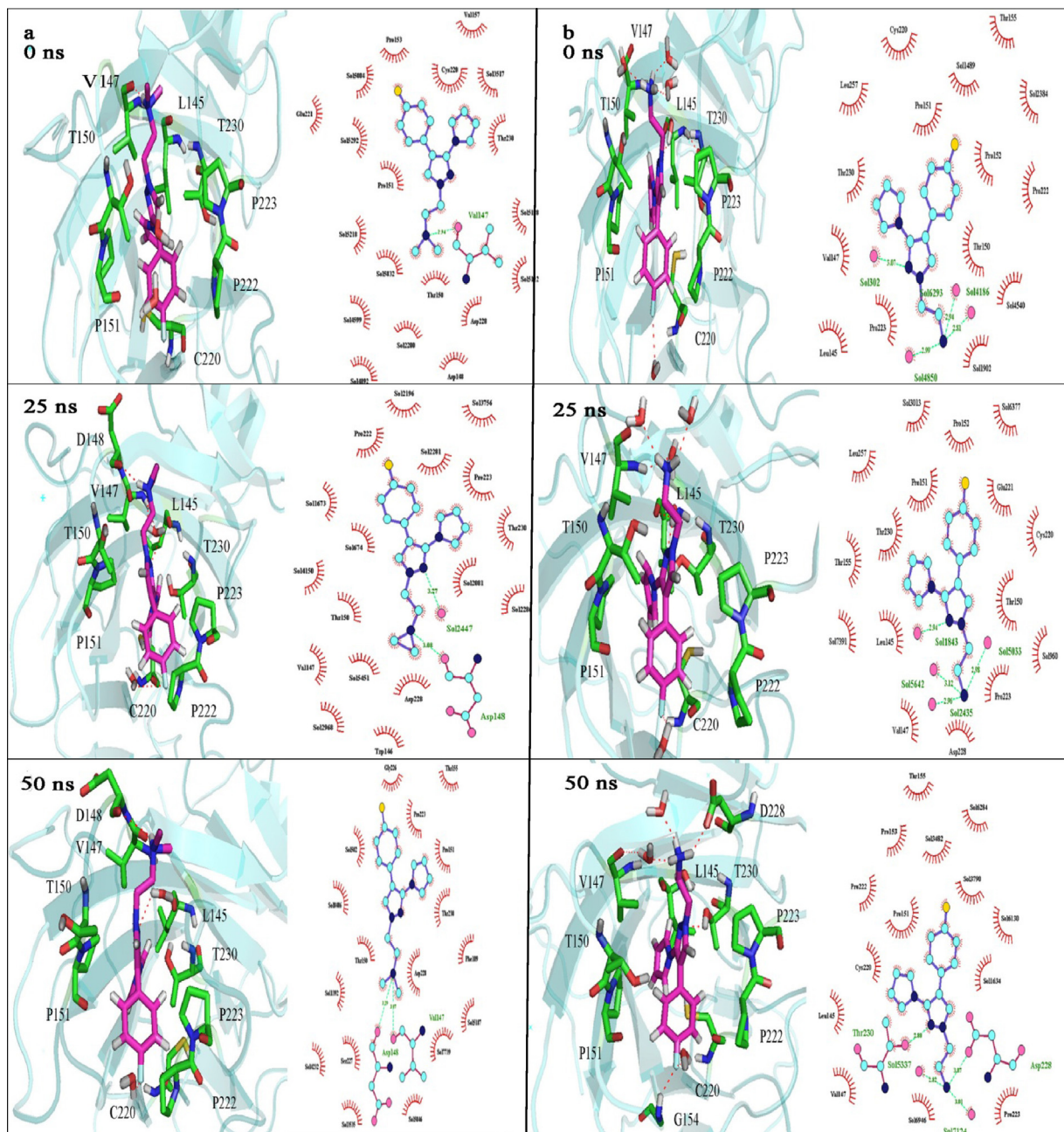


Fig. 10. 2D and 3D plots of the interaction between two ligands and p53 at different times during the MD simulation. (column a) The interaction of PK7242 with p53. (column b) The interaction of the ligand 3 with p53.

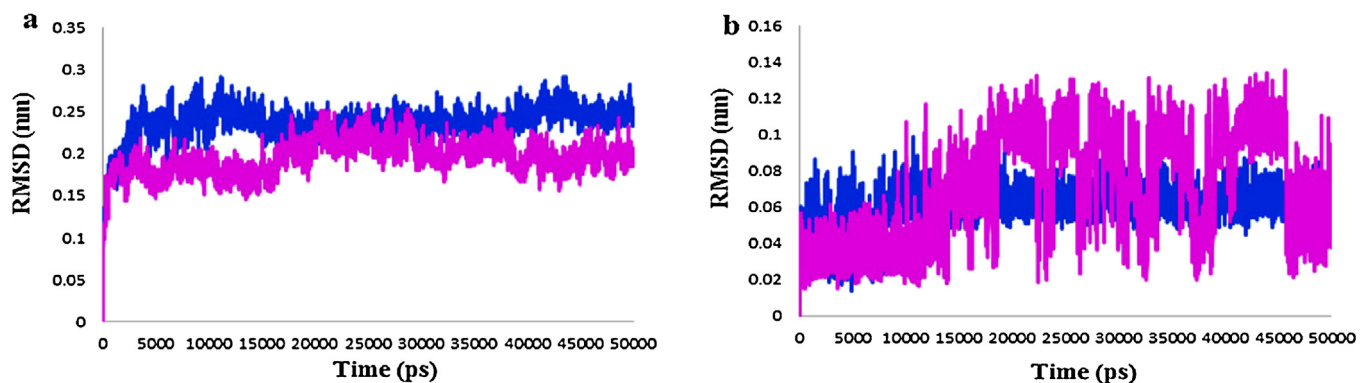


Fig. 11. The RMSD profile. (a) Hsp90 backbone in complex with inhibitor 2 (magenta), ligand 3 (blue). (b) Inhibitor 2 (magenta), ligand 3 (blue) as a function of simulation time.

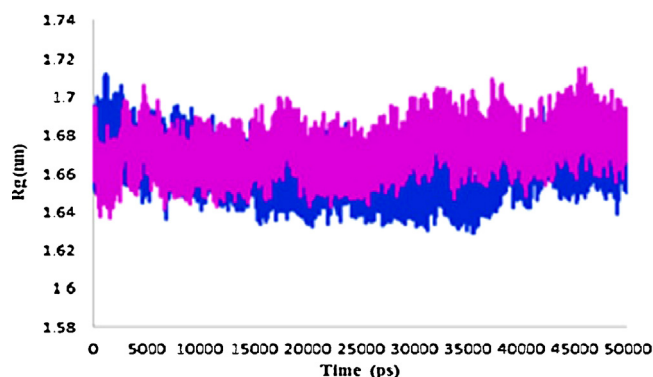


Fig. 12. The gyration radius plot of backbone. Inhibitor 2 (magenta) and ligand 3 (blue).

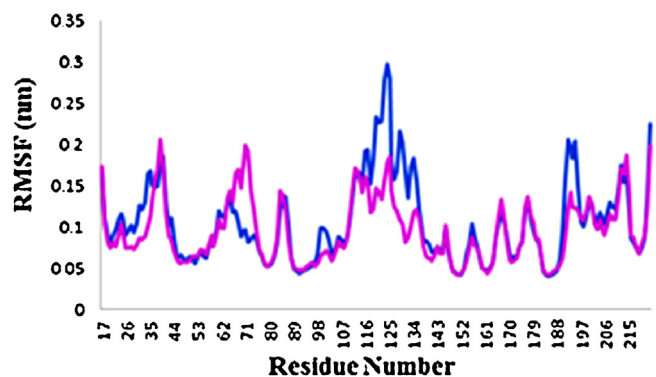


Fig. 13. The RMSF plot. Hsp90-inhibitor 2 (magenta) and Hsp90-ligand 3 (blue).

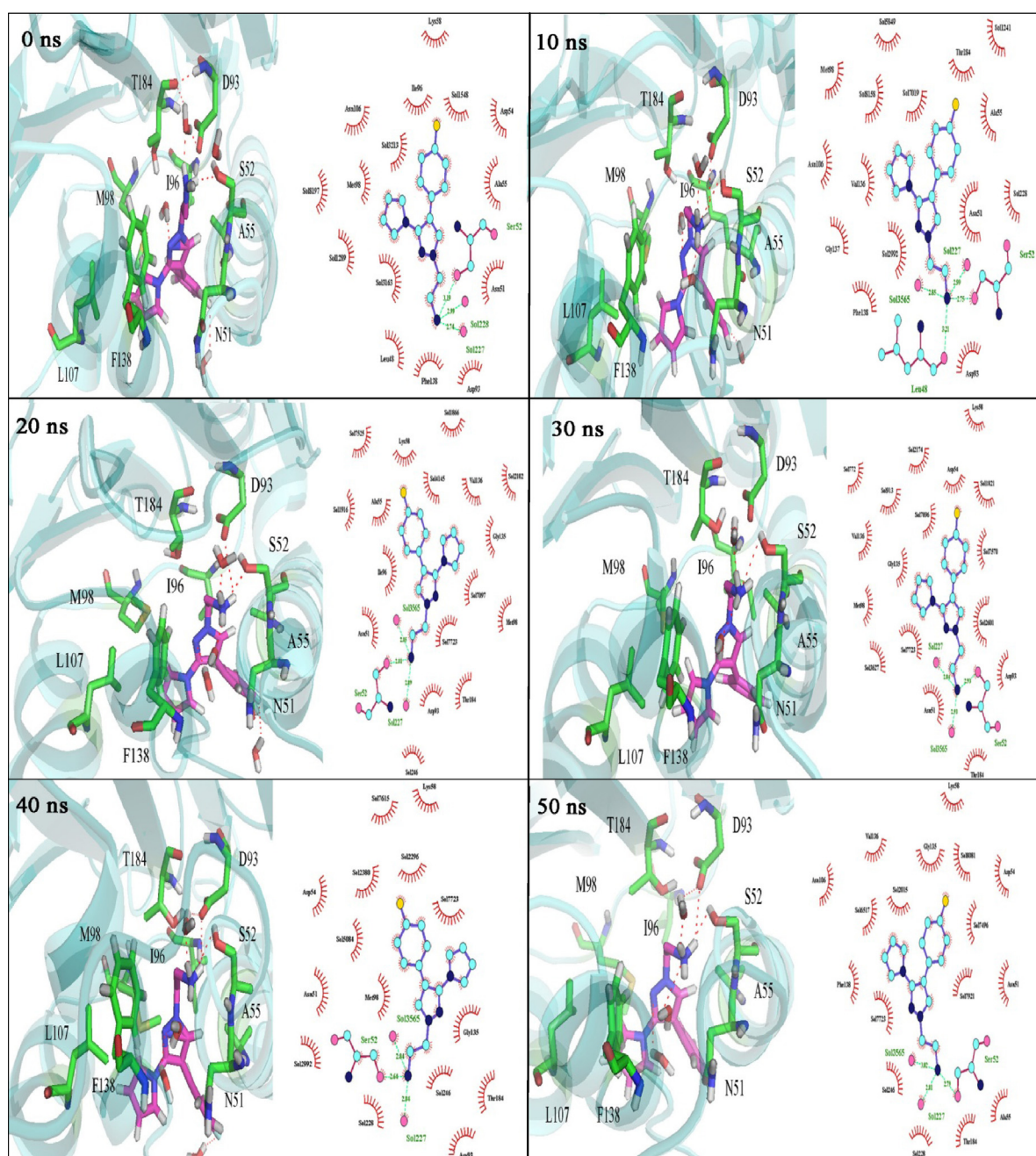


Fig. 14. 2D and 3D plots of the interaction between ligand and Hsp90. 2D and 3D plots of the interactions between ligand 3 and Hsp90 at different times during the MD simulation (0, 10, 20, 30, 40, 50 ns).

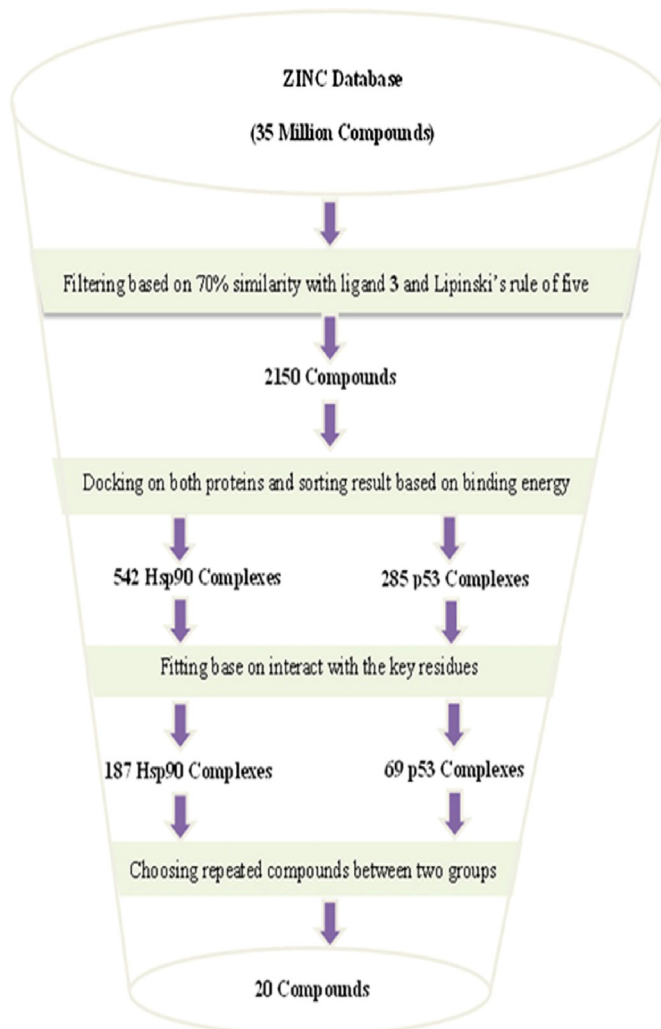


Fig. 15. Representation of the overall filtering process in VS.

The molecular docking of the newly proposed ligand 3 with both proteins (p53 and Hsp90) was carried out. In the p53-ligand complex 3, the N atom in the pyrazole ring interacted with Leu145 and Thr230 by the structural water molecule, with the same distance and binding energy in PK7242 ligand. In the Hsp90-ligand 3 complex, the evaluation of results shows that ligand 3 (docking energy of -6.45 kcal/mol) was more stable than PK7242 (docking energy of -5.61 kcal/mol). The distance between the hydrogen of terminal amine and Asp93 was 2.54 \AA and between the structural water molecules and Asp93 was 2.22 \AA . The main hydrophobic and hydrophilic interactions in both proteins are shown in Fig. 6.

According to the docking results, ligand 3 can be proposed as a dual agent, with an inhibitory effect on Hsp90 and an activatory effect on mutant p53.

3.2. MD simulation analysis

The MD simulation was carried out to ensure the stability of ligand 3 in the active site of proteins and also to compare its interaction modes of PK7242 and inhibitor 2 with p53 and Hsp90, respectively [31]. The docking's best conformation was chosen to carry out MD simulations (in terms of the lowest binding energy and the best orientation of the ligand in the active site). Four systems were simulated separately: Hsp90 with ligand 3 and inhibitor 2, p53 with ligand 3 and activator PK7242. After 50 ns simulations, the time-dependent conduct of MD trajectories, including

root mean square deviation (RMSD) for all backbone atoms and ligands, average fluctuations of the residues (RMSF) and gyration radius (R_g), were analyzed for all complexes.

As a function of time, the RMSD of backbone atoms was computed to evaluate the conformational stability of the protein during the simulation with a 10 ps time interval. To confirm that ligand 3 activated the mutant p53, the RMSD of backbone atoms between complexes of p53-PK7242 and p53-ligand 3 was compared. As can be seen in Fig. 7a, the RMSD profile in the two complexes was almost the same, and it was perfectly superimposed in the first 3 ns and between 8 ns to 22 ns and 28 ns to 34 ns. During the simulation, variations of RMSD was not very significant (0.3 nm in ligand PK7242 and 0.2 nm in ligand 3), which suggests that both complexes were stable under the given simulation conditions. The ligand RMSD profile in Fig. 7b shows that ligand 3 was fit in the active site and stabilized. The RMSD variations were less than 0.1 nm in ligand 3. The compactness of the protein was considered by the gyration radius (R_g). The R_g value of both complexes was nearly the same and their continuity was maintained during the simulation, as depicted in Fig. 8. The variations of protein flexibility were recognized by the root mean square fluctuation (RMSF) of backbone residues. As is shown in Fig. 9, in both systems a noticeable value of RMSF is seen in the first five residues. The fluctuations in both complexes were the same; except in residues 136–156. This indicates that these regions of protein in the ligand 3 were more stable than the ligand PK7242 during MD simulation. This can be ascribed to the presence of these residues in the active site of protein.

To explore the conformations and interactions of ligand 3 and PK7242 during simulation, 2D plots of the different times of simulation were obtained by LigPlot + v.1.4.5. Fig. 10 shows the comparison of 2D and 3D between the ligand 3 and PK7242 in the active site of p53 during 0, 25 and 50 ns of the simulation (a, b columns). At the beginning of simulation, the terminal amine group of the ligand PK7242 formed hydrogen bond with Val147 whereas in the ligand 3, the hydrogen bond was made with crystallography water molecules. The N atom of pyrazole ring made hydrogen bond with Leu145 via the structural water molecule. In both complexes, the residues Val147, Thr150, Pro151, Cys220, Pro222, and Pro 223 perched around the ligand. After 25 ns, the terminal amine group formed two hydrogen bonds with Asp148 and structural water molecule, and N atom in pyrazole ring made hydrogen bond with Leu147 via structural water molecule in the ligand PK7242. Four hydrogen bonds were created between the ligand 3 and the water molecules and two hydrogen bonds were made with Val147 and Leu145 via two molecules of water. On the other side of both ligands, F atom created hydrogen bond with the water molecule. Finally, at the end of the simulation (50 ns), hydrogen bonds were created between the terminal amine group of PK7242 with Asp148 and Val147. The N atom of pyrazole ring and F atom made hydrogen bond with structural water molecules. In the case of ligand 3, the terminal amine group made H-bond with two waters and Asp228. Val147 was involved in the hydrogen bond via the crystallography water molecule. Two water molecules participated in the hydrogen bond with the N atom of pyrazole ring and F. The F atom also made the hydrogen bond with Gly154. As is shown in Fig. 10, the both complexes perched in the center of active site of p53. According to the MD simulation analysis and also the comparison of the interactions between ligand 3 and PK7242 with p53, elimination of dimethyl moiety did not vary the activatory effect on mutant p53.

The analysis of MD simulation of Hsp90 complexes revealed that the RMSD plot of Hsp90-ligand 3 and Hsp90-inhibitor 2 were matched fully between 16 ns and 28 ns simulation, as demonstrated in Fig. 11a. Variations of RMSD were not very significant, which imply the stability of both complexes. A comparison between the RMSD plots show that the Hsp90-ligand 3 system was stable after

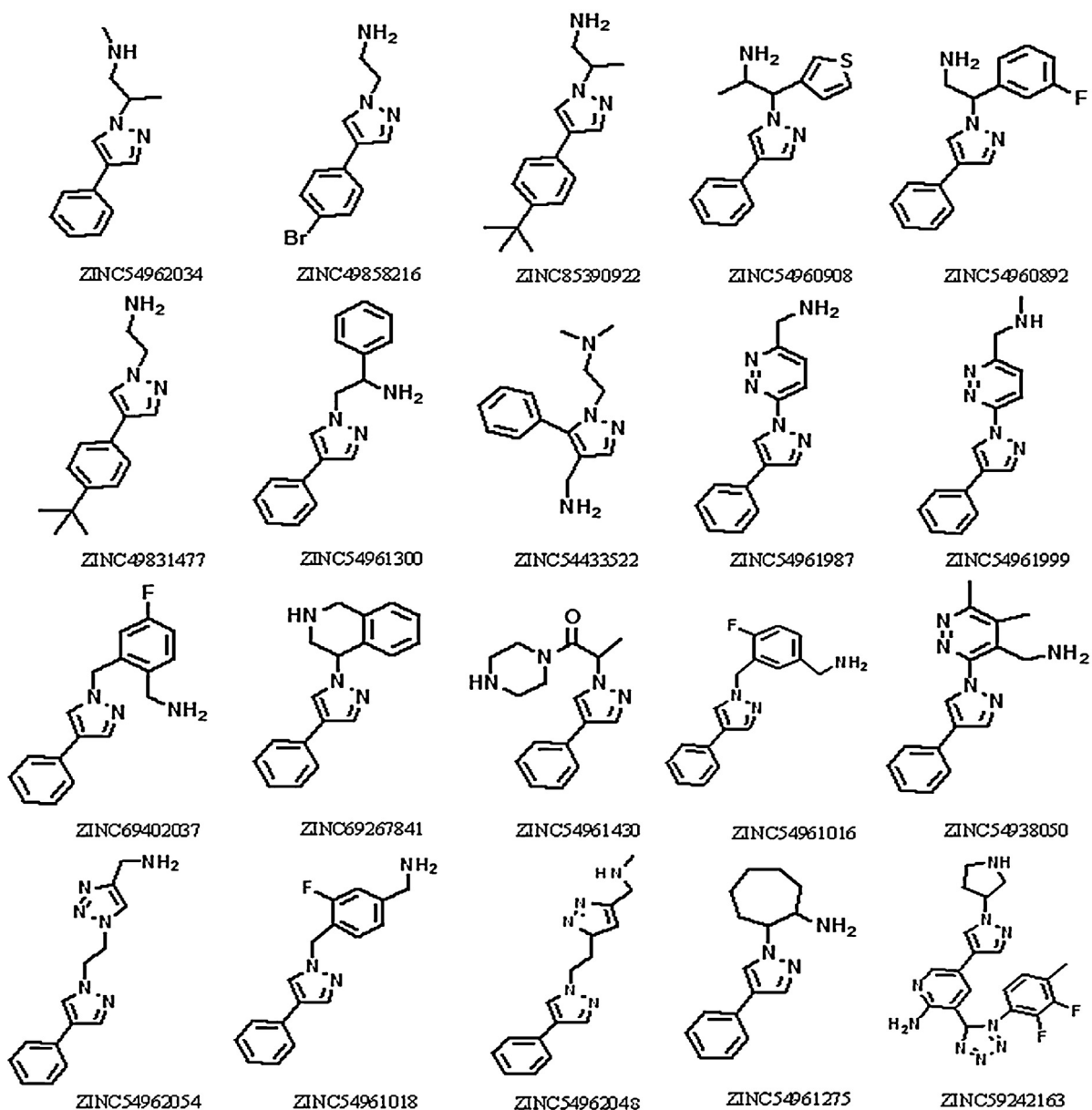


Fig. 16. The obtained compounds of VS. 20 compounds, which interact with the key residues of both proteins (Hsp90 and p53), were obtained.

2 ns but the Hsp90-inhibitor 2 reached a stable level very fast (500 ps). By investigating the RMSD plots of two ligands (Fig. 11b), it can be observed that both of the ligands were also fit in the active site and stabilized. During of simulation, the RMSD of ligand 3 stayed stable but the RMSD of inhibitor 2 changed and sometimes it were superimposed with ligand 3. In the last 5 ns (45–50 ns), the RMSD of both of them were superimposed. The RMSD analysis of ligand 3 indicates that this ligand had a significant stability in the active site during the MD simulation. The Rg plot is presented in Fig. 12. The Rg value of ligand 3 and the inhibitor 2 were superimposed and the continuity of both complexes was maintained during the simulation. As is shown in Fig. 13, the RMSF values were almost the same in both systems. In residues 65–75, the fluctuation of inhibitor 2 was higher than ligand 3 which reveal that ligand 3 was more stable than inhibitor 2 in this part. In residues 97–102 and 187–197, the fluctuation of ligand 3 was higher than inhibitor 2. In residues 115–135 the fluctuation was high, which indicates that these parts of the protein were more unstable than other parts during the MD simulation, especially in the ligand 3. In both lig-

ands, the residues 40–65, 75–98, 104–115, 143–188, 195–223 were superimposed that these parts were the key residues in the active site.

The MD simulation analysis shows that ligand 3 is stable in the active site of Hsp90. 3D and 2D plots of the different times of simulation were obtained to evaluate the conformations and interactions of ligand 3 during simulation. Fig. 14 shows the interaction of ligand 3 within the active site during 0, 10, 20, 30, 40 and 50 ns of the simulation. At the beginning of the simulation (0 time), four hydrogen bonds were formed between the terminal amino group and Ser52, Asp93, and two structural water molecules. Also, one hydrogen bond between N atom of pyrazole ring and a structural water molecule was formed. The structural water molecule was observed between ligand, Asp93 and Thr184 that can be created hydrogen bond. During the first 20 ns, the terminal amino group made H-bond with Asp93, Ser52 and two molecules of water. In addition, two structural water molecules created hydrogen bond with the N atom of pyrazole ring and F. But in 30 ns, only three hydrogen bonds were seen with Ser52 and two molecules of water.

At this time, the orientation of the terminal amino group of ligand changed and the distance between Asp93 and water molecule was increased so that the hydrogen bond did not form but the ligand was still in the active site. During the last 20 ns (40 and 50 ns), the interaction between Asp93 and ligand was again created. According to Fig. 14 it can be concluded, ligand 3 was stable in the active site with hydrophobic and hydrophilic interactions and did not move to outside of active site during the simulation.

3.3. Virtual screening study

By the docking method and MD simulation, ligand 3 was introduced as a Hsp90 inhibitor and a mutant p53 activator. To predict other dual agents, like ligand 3, a structure-based virtual screening (VS) was performed over a library of ZINC database. A library with 2150 compounds was obtained based on a 70% similarity with ligand 3 and Lipinski's "rule of five" namely: molecular weight <500, number of H-bond donors <5, number of H-bond acceptors <10 and partition coefficient $\log P < 5$ [18,32]. Docking runs were performed for each compound with both proteins. The docking results were sorted by binding energy. 542 Hsp90 complexes and 285 p53 complexes were obtained. Respectively, 187 and 69 compounds formed good interactions with the key residues and were fit in the Hsp90 and p53 active site. The goal was to predict dual agents, so the same compounds were selected from the two groups. The flowchart of the overall performed VS is shown in Fig. 15. Eventually, 20 compounds which interacted with the key residues of both proteins (Hsp90 and p53) were obtained, as displayed in Fig. 16.

In all of the introduced compounds, the terminal amino group (aliphatic or cyclic) with one or two free hydrogen atoms existed, which could form a hydrogen bond with Asp93 in Hsp90. These compounds show that substitution of pyrrole ring or any other group at position 3 of pyrazole ring is not necessary for the key interactions in the two proteins, but phenyl segment at position 4 or 5 of pyrazole ring is important for hydrophobic interactions in both of them.

4. Conclusion

The PK7242 ligand is an activator of mutant p53 with a pyrazole scaffold. This moiety also exists in some of the Hsp90 inhibitors. According to the structure of PK7242, ligand 3 with a pyrazole scaffold was predicted as a dual agent (the inhibitor of the Hsp90 and the activator of mutant p53). Molecular dynamic simulation analyses such as RMSD, RMSF and Rg, showed that ligand 3, is stable in the Hsp90 and p53 active sites. A new library similar to predicted ligand was generated from ZINC database. A structure-based virtual screening was done and 20 compounds were predicted as dual agents. In all of the introduced compounds, the amino group with one or two free hydrogen atoms existed. These compounds show that pyrrole moiety is not necessary for the key interactions, but phenyl segment is an important element for hydrophobic interactions in both proteins.

Acknowledgment

We gratefully acknowledge the financial support from Tehran University of Medical Sciences.

References

- [1] S. Sakkiah, S. Thangapandian, S. John, K.W. Lee, Pharmacophore based virtual screening, molecular docking studies to design potent heat shock protein 90 inhibitors, *Eur. J. Med. Chem.* 46 (2011) 2937–2947.
- [2] J.R. McConnell, S.R. McAlpine, Heat shock proteins 27, 40, and 70 as combinational and dual therapeutic cancer targets, *Bioorg. Med. Chem. Lett.* 23 (2013) 1923–1928.
- [3] A.J. Massey, D.S. Williamson, H. Browne, J.B. Murray, P. Dokurno, T. Shaw, A.T. Macias, Z. Daniels, S. Geoffroy, M. Dopson, A novel, small molecule inhibitor of Hsc70/Hsp70 potentiates Hsp90 inhibitor induced apoptosis in HCT116 colon carcinoma cells, *Cancer Chemother. Pharmacol.* 66 (2010) 535–545.
- [4] S.H. McLaughlin, F. Sobott, Z.-p Yao, W. Zhang, P.R. Nielson, J.G. Grossmann, E.D. Laue, C.V. Robinson, S.E. Jackson, The co-chaperone p23 arrests the Hsp90 ATPase cycle to trap client proteins, *J. Mol. Biol.* 356 (2006) 746–758.
- [5] S. Verma, A. Singh, A. Mishra, Dual inhibition of chaperoning process by taxifolin: molecular dynamics simulation study, *J. Mol. Graphics Modell.* 37 (2012) 27–38.
- [6] G. Chiosis, M.N. Timaul, B. Lucas, P.N. Munster, F.F. Zheng, L. Sepp-Lorenzino, N. Rosen, A small molecule designed to bind to the adenine nucleotide pocket of Hsp90 causes Her2 degradation and the growth arrest and differentiation of breast cancer cells, *Chem. Biol.* 8 (2001) 289–299.
- [7] A.S. Sreedhar, K. Mihály, B. Pató, T. Schnaider, A. Steták, K. Kis-Petik, J. Fidy, T. Simonic, A. Maráz, P. Csermely, HSP90 inhibition accelerates cell lysis anti-HSP90 ribozyme reveals a complex mechanism of HSP90 inhibitors involving both superoxide-and HSP90-dependent events, *J. Biol. Chem.* 278 (2003) 35231–35240.
- [8] F. Hagn, S. Lagleder, M. Retzlaff, J. Rohrberg, O. Demmer, K. Richter, J. Buchner, H. Kessler, Structural analysis of the interaction between Hsp90 and the tumor suppressor protein p53, *Nat. Struct. Mol. Biol.* 18 (2011) 1086–1093.
- [9] H. Horn, K. Vousden, Coping with stress: multiple ways to activate p53, *Oncogene* 26 (2007) 1306–1316.
- [10] C. Wang, J. Chen, Phosphorylation and hsp90 binding mediate heat shock stabilization of p53, *J. Biol. Chem.* 278 (2003) 2066–2071.
- [11] N. Rivlin, R. Brosh, M. Oren, V. Rotter, Mutations in the p53 tumor suppressor gene important milestones at the various steps of tumorigenesis, *Genes Cancer* 2 (2011) 466–474.
- [12] P. Müller, P. Ceskova, B. Vojtesek, Hsp90 is essential for restoring cellular functions of temperature-sensitive p53 mutant protein but not for stabilization and activation of wild-type p53 implications for cancer therapy, *J. Biol. Chem.* 280 (2005) 6682–6691.
- [13] F.M. Boeckler, A.C. Joerger, G. Jaggi, T.J. Rutherford, D.B. Veprintsev, A.R. Fersht, Targeted rescue of a destabilized mutant of p53 by an in silico screened drug, *Proc. Natl. Acad. Sci. U. S. A.* 105 (2008) 10360–10365.
- [14] X. Liu, R. Wilcken, A.C. Joerger, I.S. Chuckowree, J. Amin, J. Spencer, A.R. Fersht, Small molecule induced reactivation of mutant p53 in cancer cells, *Nucleic Acids Res.* 41 (2013) 6034–6044.
- [15] T. Ganesh, P. Thepchatri, L. Li, Y. Du, H. Fu, J.P. Snyder, A. Sun, Synthesis and SAR study of N-(4-hydroxy-3-(2-hydroxynaphthalene-1-yl)phenyl)-arylsulfonamides: heat shock protein 90 (Hsp90) inhibitors with submicromolar activity in an *in vitro* assay, *Bioorg. Med. Chem. Lett.* 18 (2008) 4982–4987.
- [16] K.-M.J. Cheung, T.P. Matthews, K. James, M.G. Rowlands, K.J. Boxall, S.Y. Sharp, A. Maloney, S.M. Roe, C. Prodromou, L.H. Pearl, The identification, synthesis, protein crystal structure and *in vitro* biochemical evaluation of a new 3,4-diarylpyrazole class of Hsp90 inhibitors, *Bioorg. Med. Chem. Lett.* 15 (2005) 3338–3343.
- [17] J. Travers, S. Sharp, P. Workman, HSP90 inhibition: two-pronged exploitation of cancer dependencies, *Drug Discov. Today* 17 (2012) 242–252.
- [18] J.J. Irwin, T. Sterling, M.M. Mysinger, E.S. Bolstad, R.G. Coleman, ZINC: a free tool to discover chemistry for biology, *J. Chem. Inf. Model.* 52 (2012) 1757–1768.
- [19] G.M. Morris, R. Huey, W. Lindstrom, M.F. Sanner, R.K. Belew, D.S. Goodsell, A.J. Olson, AutoDock4 and AutoDockTools4: automated docking with selective receptor flexibility, *J. Comput. Chem.* 30 (2009) 2785–2791.
- [20] J. Wang, W. Wang, P.A. Kollman, D.A. Case, Automatic atom type and bond type perception in molecular mechanical calculations, *J. Mol. Graphics Modell.* 25 (2006) 247–260.
- [21] H. Azizian, H. Bahrami, P. Pasalar, M. Amanlou, Molecular modeling of *Helicobacter pylori* arginase and the inhibitor coordination interactions, *J. Mol. Graphics Modell.* 28 (2010) 626–635.
- [22] S. Cosconati, S. Forli, A.L. Perryman, R. Harris, D.S. Goodsell, A.J. Olson, Virtual screening with Autodock: theory and practice, *Expert Opin. Drug Discov.* 5 (2010) 597–607.
- [23] G.M. Morris, D.S. Goodsell, R.S. Halliday, R. Huey, W.E. Hart, R.K. Belew, A.J. Olson, Automated docking using a Lamarckian genetic algorithm and an empirical binding free energy function, *J. Comput. Chem.* 19 (1998) 1639–1662.
- [24] S. Pronk, S. Päll, R. Schulz, P. Larsson, P. Bjelkmar, R. Apostolov, M.R. Shirts, J.C. Smith, P.M. Kasson, D. van der Spoel, GROMACS 4.5: a high-throughput and highly parallel open source molecular simulation toolkit, *Bioinformatics* (2013), btt 055.
- [25] A.W. Schuttelkopf, D.M. Van Aalten, PRODRG: a tool for high-throughput crystallography of protein-ligand complexes, *Acta Crystallogr. D: Biol. Crystallogr.* 60 (2004) 1355–1363.
- [26] M. Frisch, G. Trucks, H. Schlegel, G. Scuseria, M. Robb, J. Cheeseman, V. Zakrzewski, J. Montgomery Jr., R. Stratmann, J. Burant, Gaussian 98, Revision A.7, Gaussian, Inc., Pittsburgh, PA, 1998, pp. 12.
- [27] C.R. Sondergaard, M.H. Olsson, M. Rostkowski, J.H. Jensen, Improved treatment of ligands and coupling effects in empirical calculation and rationalization of pK_a values, *J. Chem. Theory Comput.* 7 (2011) 2284–2295.
- [28] K. Bagherzadeh, F. Shirgahi Talari, A. Sharifi, M.R. Ganjali, A.A. Saboury, M. Amanlou, A new insight into mushroom tyrosinase inhibitors: docking,

- pharmacophore-based virtual screening, and molecular modeling studies, *J. Biomol. Struct. Dyn.* (2014) 1–15.
- [29] H. Azizian, F. Nabati, A. Sharifi, F. Siavoshi, M. Mahdavi, M. Amanlou, Large-scale virtual screening for the identification of new helicobacter pylori urease inhibitor scaffolds, *J. Mol. Model.* 18 (2012) 2917–2927.
- [30] M. Bruncko, S.K. Tahir, X. Song, J. Chen, H. Ding, J.R. Huth, S. Jin, R.A. Judge, D.J. Madar, C.H. Park, *N*-Aryl-benzimidazolones as novel small molecule HSP90 inhibitors, *Bioorg. Med. Chem. Lett.* 20 (2010) 7503–7506.
- [31] X. Barril, M.C. Beswick, A. Collier, M.J. Drysdale, B.W. Dymock, A. Fink, K. Grant, R. Howes, A.M. Jordan, A. Massey, 4-Amino derivatives of the Hsp90 inhibitor CCT018159, *Bioorg. Med. Chem. Lett.* 16 (2006) 2543–2548.
- [32] C.A. Lipinski, F. Lombardo, B.W. Dominy, P.J. Feeney, Experimental and computational approaches to estimate solubility and permeability in drug discovery and development settings, *Adv. Drug Deliv. Rev.* 64 (2012) 4–17.